

# A Generic Self-Assembly Process in Microcompartments and Synthetic Protein Nanotubes

Ismail Uddin, Stefanie Frank, Martin J. Warren, and Richard W. Pickersgill\*

**Bacterial microcompartments enclose a biochemical pathway and reactive intermediate within a protein envelope formed by the shell proteins. Herein, the orientation of the propanediol-utilization (Pdu) microcompartment shell protein PduA in bacterial microcompartments and in synthetic nanotubes, and the orientation of PduB in synthetic nanotubes are revealed. When produced individually, PduA hexamers and PduB trimers, tessellate to form flat sheets in the crystal, or they can self-assemble to form synthetic protein nanotubes in solution. Modelling the orientation of PduA in the 20 nm nanotube so as to preserve the shape complementarity and key interactions seen in the crystal structure suggests that the concave surface of the PduA hexamer faces out. This orientation is confirmed experimentally in synthetic nanotubes and in the bacterial microcompartment produced *in vivo*. The PduB nanotubes described here have a larger diameter, 63 nm, with the concave surface of the trimer again facing out. The conserved concave surface out characteristic of these nano-structures reveals a generic assembly process that causes the interface between adjacent subunits to bend in a common direction that optimizes shape complementarity and minimizes steric clashes. This understanding underpins engineering strategies for the biotechnological application of protein nanotubes.**

Bacterial microcompartments are proteinaceous organelles found in a wide range of bacterial phyla, they comprise a protein shell encapsulating an enzymatic core and contain a reactive intermediate. The propanediol-utilization (Pdu) microcompartment is comprised of eight shell proteins forming a closed capsule 100–150 nm across which encapsulates a number of enzymes including: diol-dehydratase and propanol

dehydrogenase. The eight shell proteins fall into three families: hexamers, trimers, and pentamers, which form a pleomorphic pseudo-icosahedral shell around the condensed enzymes.<sup>[1–3]</sup> PduA, a major shell protein, tessellates in the crystal lattice and when produced on its own, self-assembles into nanotubes.<sup>[4–6]</sup>


Nanotubes, comprising the hexameric bacterial microcompartment protein PduA, assemble spontaneously *in vitro* once the salt concentration is reduced below 0.05 M (Figure 1a). These nanotubes, of fixed diameter 20 nm and variable length, are thought to assemble in the same way as the flat sheets of tessellated hexamer subunits seen in the crystal. To form a tube, rather than a flat sheet, either the hexamer is distorted or the interface between hexamers is bent. The rather fragile interface, dominated by electrostatic rather than hydrophobic interactions, appears much easier to bend than the hexamers themselves (Figure 1b), so our models are based on making a bend

at the interface in such a way as to preserve the characteristic hydrogen-bonding of the antiparallel lysine pair of PduA shown to be essential for nanotube formation (Figure 1c). We have previously proposed two basic models of nanotubes: zigzag with the flat edge of the hexamer subunit approximately parallel to the tube axis and with 10 hexamers per turn with a bend angle of 36° (Figure 1d) and armchair with the flat edge perpendicular to the tube axis 12 hexamers per turn with a bend angle of 30° (Figure 1e).<sup>[5]</sup> Another possibility, close in architecture to the zigzag is a single-start helical model with 10 hexamers per turn, a bend angle of 37.5° and pitch 61 nm (Figure 1f). However, these models do not provide an answer to the question of which face of the hexamer is accessible to the lumen of the nanotube and which side is out (Figure 1g)? Here, we used several criteria to assess the direction of the bend *in silico* including monitoring the lysine interaction, measuring hydrophobic burial, and counting protein clashes, it is the latter that gave the clearest prediction of preferred bend angle (Figure 1h,i; also see Figure 1b).<sup>[7–10]</sup> Both models preserve the lysine interaction across the two distinct interfaces generated when the hexamers are bent to form a ring and when rings stack to form a tube, but the zigzag model with the concave surface facing out gave minimal clashes compared to the opposite bend angle and either bend angle with the armchair model (Figure 1h,j). It is for this reason that we favor the zigzag model or the closely related single start helix model with concave surface facing out. Of these two, the helical model has the bend axis most

I. Uddin, Prof. R. W. Pickersgill  
 School of Biological and Chemical Sciences  
 Queen Mary University of London  
 Mile End Road, London E1 4AA, UK  
 E-mail: r.w.pickersgill@qmul.ac.uk

Dr. S. Frank  
 Department of Biochemical Engineering  
 University College London  
 Gordon Street, London WC1E 6BT, UK

Prof. M. J. Warren  
 School of Biosciences  
 University of Kent  
 Giles Lane, Canterbury, Kent CT2 7NJ, UK

 The ORCID identification number(s) for the author(s) of this article can be found under <https://doi.org/10.1002/sml.201704020>.

© 2018 The Authors. Published by WILEY-VCH Verlag GmbH & Co. KGaA, Weinheim. This is an open access article under the terms of the Creative Commons Attribution License, which permits use, distribution and reproduction in any medium, provided the original work is properly cited.

DOI: 10.1002/sml.201704020

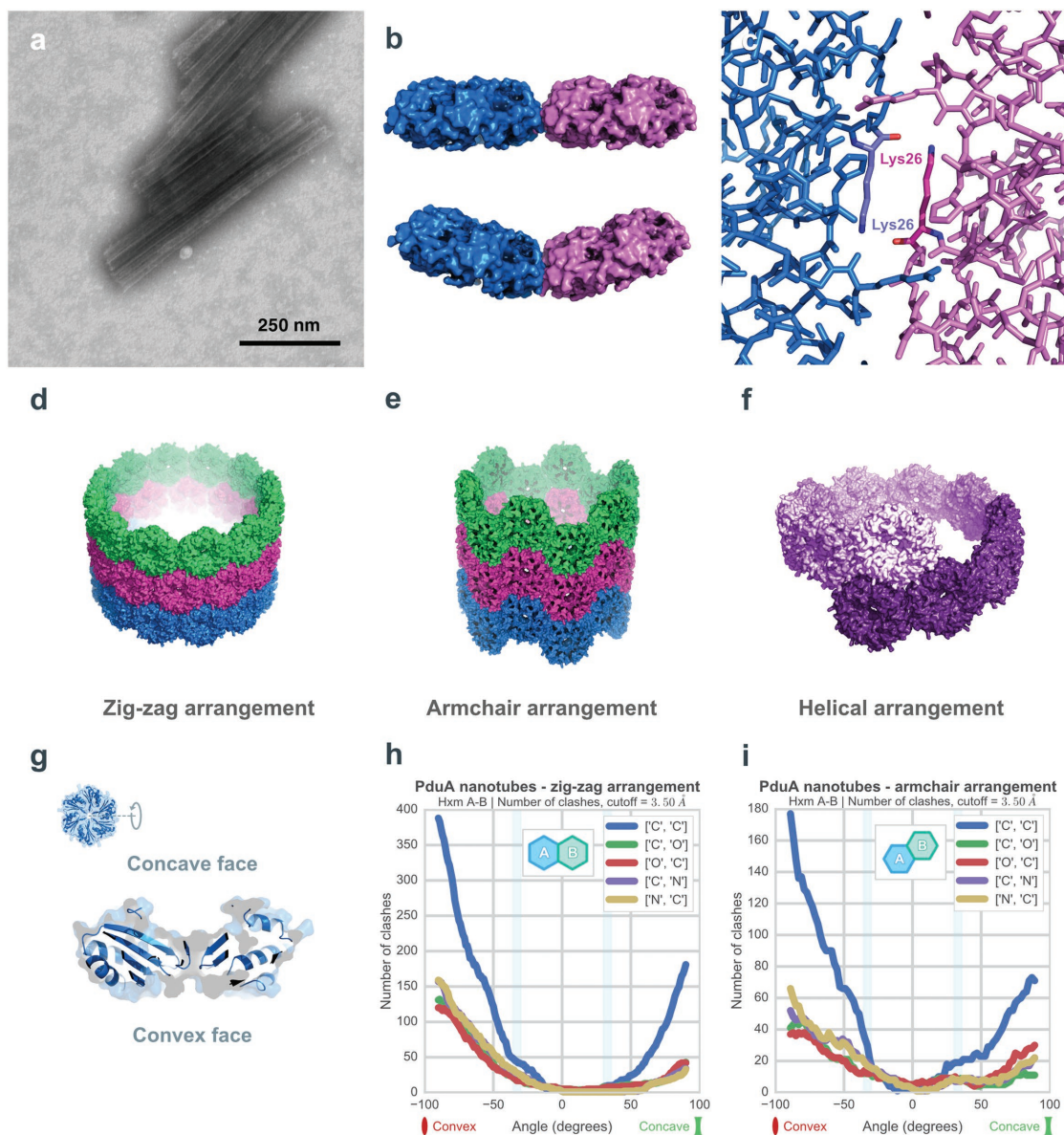


**Figure 1.** Modeling the architecture of PduA protein nanotubes based on the packing of PduA seen in the crystal. a) Transmission electron microscopic image of PduA nanotubes, consistently 20 nm in diameter. Scale bar 250 nm. b) Top-down view of two adjacent PduA hexamers, illustrating the fragile hexamer–hexamer interface, at both 0° (top) and 36° (bottom) bend angle. c) The antiparallel lysine arrangement between adjacent Lys26 residues, held together by hydrogen bonding. d–f) Zig-zag, armchair, and helical arrangement model of PduA, respectively. g) Top-down view of a PduA hexamer and cross-section (expanded), illustrating the concave and convex faces of the hexamer. The N-terminal hexahistidine tag is on the concave surface. h, i) Number of protein clashes counted at the PduA hexamer–hexamer interface, as a function of bend angle, for the zig-zag and armchair arrangement, respectively. The zig-zag or closely related helical model with concave surface facing out is preferred from the in silico modeling.

closely parallel to the edge of the hexamer. Forming a tube, rather than a flat sheet, reduces the edge-effects present in the nanostructure.

The cleavable N-terminal hexahistidine-tag of PduA used for purification of the hexamer is located on its concave surface. If the orientation of the hexamer in the proposed model is correct then the tagged PduA nanotubes should have the hexahistidine-tag available for binding to nickel nitrilotriacetic acid (Ni-NTA) beads,<sup>[11]</sup> whereas tubes formed from PduA with the tag removed (nontagged nanotubes) will be unable to bind with the same affinity. We assembled nanotubes from

both samples, added Ni-NTA magnetic beads and assessed the release of the nanotubes from the Ni-NTA beads after unbound nanotubes (due to heavy loading) had been washed off. The tagged PduA tubes were bound as judged from their release at 0.15 M and higher imidazolium concentrations (Figure 2a), but the nontagged nanotubes failed to bind to the Ni-NTA beads (Figure 2b). This provides clear evidence that the N-terminus of the protein is available for binding, thereby supporting the calculations showing that the concave surface of PduA faces out. The eluted tubes were subsequently imaged using electron microscopy. This result was substantiated by imaging small

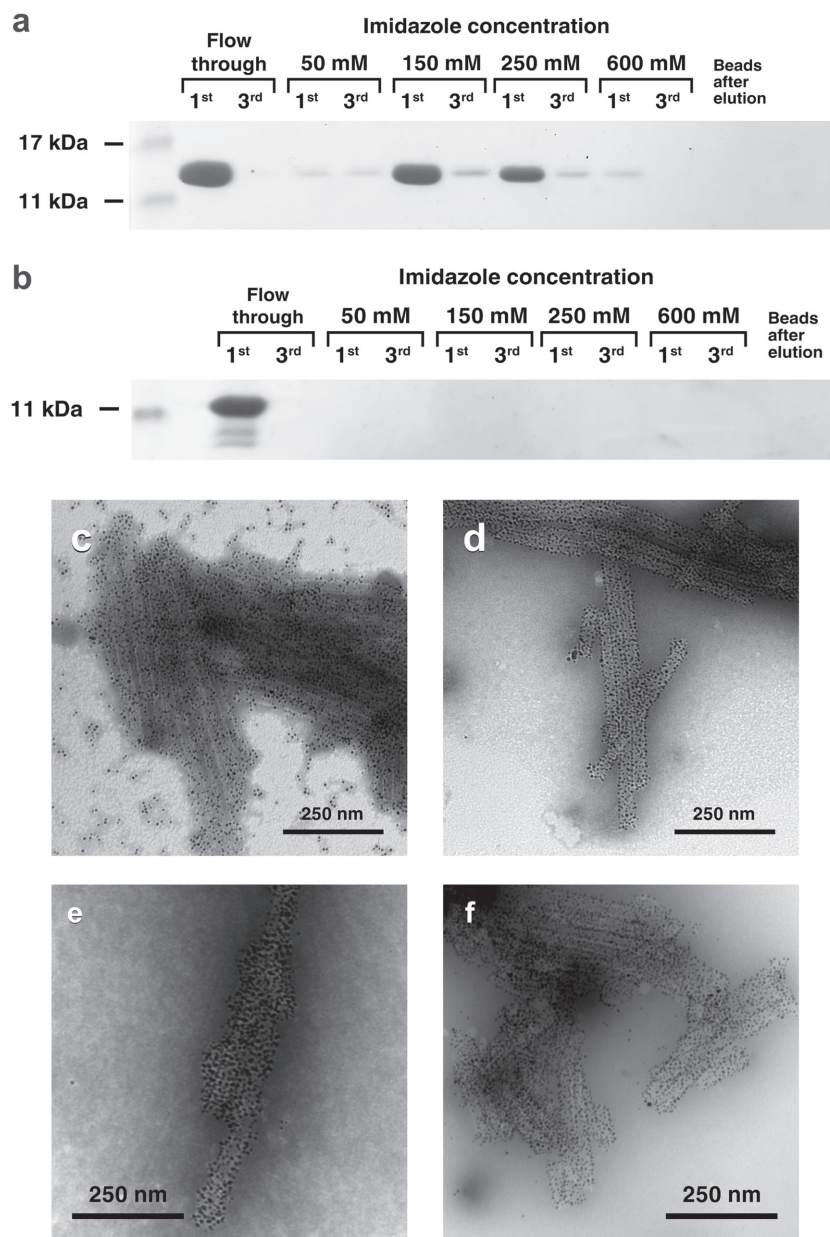


**Figure 2.** Evidence concerning the orientation of PduA hexamers in protein nanotubes. a) SDS PAGE gel demonstrating the binding and release of hexahistidine tagged PduA nanotubes from Ni-NTA magnetic beads. The beads were heavily loaded with nanotubes and the first pair of lanes shows the flow-through, a considerable quantity of tubes were washed off in the first wash, none in the third (final) wash of the beads. Subsequent pairs of lanes show the elution in increasing imidazole concentrations. Again, the first and final washes are presented. There was no significant elution at 0.05 M imidazole. The nanotubes started to elute at 0.15 M imidazole. b) SDS PAGE gel for the control experiment, demonstrating the lack of binding of nontagged PduA nanotubes. The nanotubes all appear in the flow-through, none are eluted or remain on the beads. c) Transmission electron microscopic images of tagged PduA nanotubes binding gold nanoparticles in the presence of 0.25 M imidazole. d) Transmission electron microscopic images of nontagged PduA nanotubes binding gold nanoparticles in the presence of 0.25 M imidazole. The binding of nanoparticles is tighter and more precise to the less-flexible N-terminal sequence GSH formed after cleavage of the external histidine-tag than to the longer and more flexible hexahistidine tag. The much larger Ni-NTA beads used in the binding and release experiment using cleaved PduA do not have access to the GSH sequence. The binding and release experiments and the nanoparticle-binding images show the concave side of PduA faces out. e) PduA H81A nanotubes with AuNPs bound under 0.25 M imidazole concentration. f) PduA H[-1]A nanotubes with AuNPs bound under 0.25 M imidazole concentration.

Ni-NTA gold nanoparticles (AuNPs) bound to the eluted nanotubes with hexahistidine tag revealing binding to the exterior of the nanotubes (Figure 2c). Far-UV circular dichroism spectroscopy reveals both the hexamers and nanotubes have  $\alpha$ -helical content, providing a direct measure of native protein structure in the protein nanotubes (Figure S1, Supporting Information).

Remarkably, when the hexahistidine tag was cleaved from the PduA hexamers the nanoparticles still bound to the nanotubes, but now the binding was more regular showing that a better-ordered binding-site had either been created or revealed (Figure 2d). Generation of the new N-terminus, sequence GSH (residues -3 to -1), on thrombin cleavage of the histidine tag would create a high-affinity binding site where the amino-terminus [-3] and imidazole side chain of His[-1] bind the nanoparticle.<sup>[12]</sup> An alternative is that more ordered binding to an accessible histidine was revealed when the hexahistidine tag was removed. His81 is the only other accessible histidine in PduA and it is in appropriate proximity with Arg79 from the adjacent hexamer in the nanotube to form a high-affinity nanoparticle binding-site. Mutating His[-1] to Ala and His81 to Ala reveals that neither residue alone is responsible for nanoparticle binding in the absence of the hexahistidine tag, so we conclude that both His[-1] and His81 form high-affinity nanoparticle-binding sites (Figure 2e,f). Note that these high-affinity binding-sites are not accessible to the affinity matrix used in the binding and release experiments and that mutation of Arg79 prevents the formation of nanotubes.

It has previously been demonstrated that overexpression of the *Citrobacter freundii* propanediol utilization microcompartment shell protein genes, *pduABJKNU*, in *Escherichia coli* produces empty bacterial microcompartments<sup>[13]</sup> and that cargo proteins can be targeted to the capsule using a specific N-terminal sequence.<sup>[14,15]</sup> Here we generated a tobacco etch virus (TEV) protease cleavable N-terminal mCherry fluorescently tagged PduA (mCherry-TEV-PduA) and coproduced it together with PduB, PduJ, PduK, PduN, and PduU to allow the formation of a shell complex.<sup>[13]</sup> By employing a rhamnose inducible TEV protease it was possible to explore the accessibility of the TEV cleavage site,<sup>[16]</sup> results which strongly indicate that the concave surface of PduA is pointing to the bacterial cytoplasm (see Figure S2 in the Supporting Information and Experimental Section for more details). In the absence of

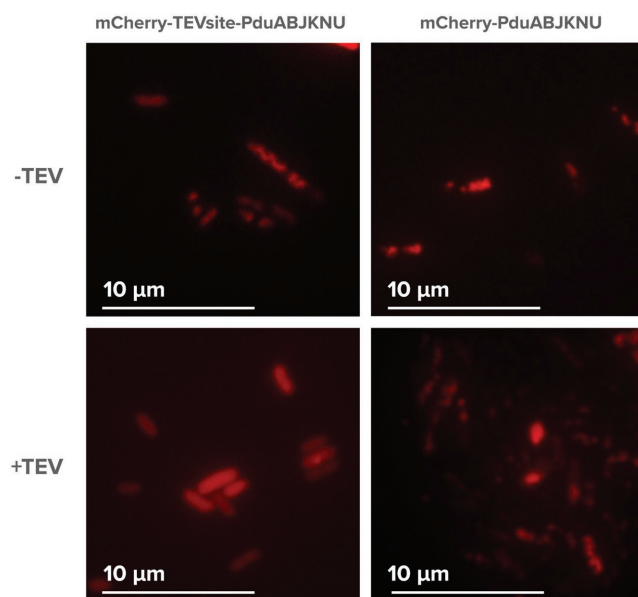


**Figure 3.** Evidence on the orientation of PduA hexamers in Pdu protein microcompartments. mCherry localization in live *E. coli* cells before (–TEV) and after (+TEV) induction of TEV protease. The strains expressing mCherry-TEVsite-PduABJKNU and the negative control mCherry-PduABJKNU were induced for 90 min, the cells were washed with fresh medium to remove inducer and stop production of more shell proteins and then the TEV protease was induced. In both strains, the mCherry signal is punctate before the production of TEV protease indicating that bacterial microcompartments are formed and mCherry is colocalized with these structures. After TEV protease has been induced for 140 min the mCherry signal is cytoplasmic in the mCherry-TEVsite-PduABJKNU-producing strain (bottom left) but appears as foci in the negative control strain lacking the TEV-cleavage site between mCherry and PduA (mCherry-PduABJKNU). These data provide clear evidence that the TEV cleavage site is on the outer surface of the microcompartment and therefore the concave surface faces out.

induced protease, the fluorescent tag is clearly punctate and associated with the microcompartments, but when the TEV protease is induced cleavage occurs and the fluorescence is no longer discrete, but spreads throughout the bacterial cytoplasm (Figure 3). In the absence of the TEV cleavable sequence, expression of the protease has no effect on the distribution of the fluorescence. Production of microcompartments was confirmed using transmission electron microscopy (TEM) (Figure S3, Supporting Information). These data provide compelling evidence that the concave surface of PduA is external in the Pdu microcompartment. The interactions involved in the tiling of PduA hexamers seen in the crystal lattice makes it clear that alternating orientations are not possible, a result underlined by atomic force microscopy (AFM) studies.<sup>[3,17]</sup>

We also discovered that the trimeric, pseudo-hexameric protein,<sup>[4,18–20]</sup> PduB<sup>[21]</sup> is capable of forming protein nanotubes when the salt concentration is lowered, but these nanotubes are larger in diameter, typically around 63 nm (Figure 4a, with statistical summary in G). In contrast to PduA, PduB nanotubes are not labeled by AuNPs (Figure 4b,c); unlike PduA the N-terminus of PduB is on the convex side, so this result is consistent with the convex side of the PduB hexamer inside, reducing accessibility of the His-tag. The algorithms used to

generate PduA nanotube models can be used to generate PduB nanotube structures with bending such that the concave surface is external, giving fewer clashes for both zigzag and arm-chair models. (Figure 4d–f,i,j; further details of the modeling are given in the Supporting Information). It is remarkable that in the crystal lattice sheets of PduB molecules do not show the precise hydrogen-bonding of antiparallel lysine pairs seen in PduA, the lysine residues are conserved, but the interaction is not, rather the interface is characterized by general shape and electrostatic complementarity. Clearly, the bend angle is shallower in these tubes and this allows for bending along the length of the tubes as a less-severe restraint is placed on the positioning of trimers along the z-axis of the tube.

The evidence from in silico and experimental studies suggest these structures have a dimpled surface appearance with the concave surface of the hexamers and trimers facing out of nanotubes and microcompartments. There is a consistent orientation and the walls of both nanotube and microcompartment structures are anticipated to be a single molecule thick. The preferred model of the nanotube is the zigzag or the closely related helical model. That the larger diameter PduB nanotubes may be able to bend along their long-axis because of the shallower bend angle between adjacent in-plane oligomers and the lack of precise lysine-lysine interaction. Although we provide clear evidence that the concave surface of the hexamers and trimers faces out, the precise organization of hexameric (PduA) and trimeric (PduB) subunits will likely be revealed by cryo-electron microscopy studies. The subunit orientation demonstrated for PduA nanotubes and the PduA hexamer in the propane-diol utilization microcompartment shell agrees with the recent crystal structure of the *Haliangium ochraceum* microcompartment shell.<sup>[22]</sup> This remarkable crystal structure of the small microcompartment shell has concave surface of the subunits facing out and the bend angles between hexamers are consistent with those predicted from our in silico modeling of PduA nanotubes.

This knowledge can be used to engineer specific protein–protein interactions to either target proteins more accurately to the lumen of microcompartments or to the outside of the filament scaffolds. To present nanobodies and enzymes on the outside, we now know to label the concave surface of these structures; and to place biochemical pathways within the lumen, they should be introduced on the convex side of the subunits forming these nanostructures.

## Experimental Section

**Protein Expression and Purification:** The expression of *C. freundii* PduA used the *pduA\** gene, which contains a mutation that knocks out the stop codon and gives an additional 23 C-terminal residues from the pET14b vector (LVKDPAAANKARKEAELAAATAEQ). The presence of these additional residues made PduA\* more soluble and easier to work with in vitro. PduA\*, referred to simply as PduA in this paper, was expressed from Bioline BL21 (DE3) cell lines. The recombinant protein was purified via immobilized metal affinity chromatography, using GE Chelating sepharose media (charged with nickel sulphate). *Lactobacillus reuteri* DSM20016 PduB was expressed from a pET-14b plasmid, in BL21 (DE3) cell lines. PduB was subsequently purified via size exclusion chromatography using a GE Sephadex S200 HR 10/30 GL column, eluting at around 14 mL, corresponding to its expected molecular

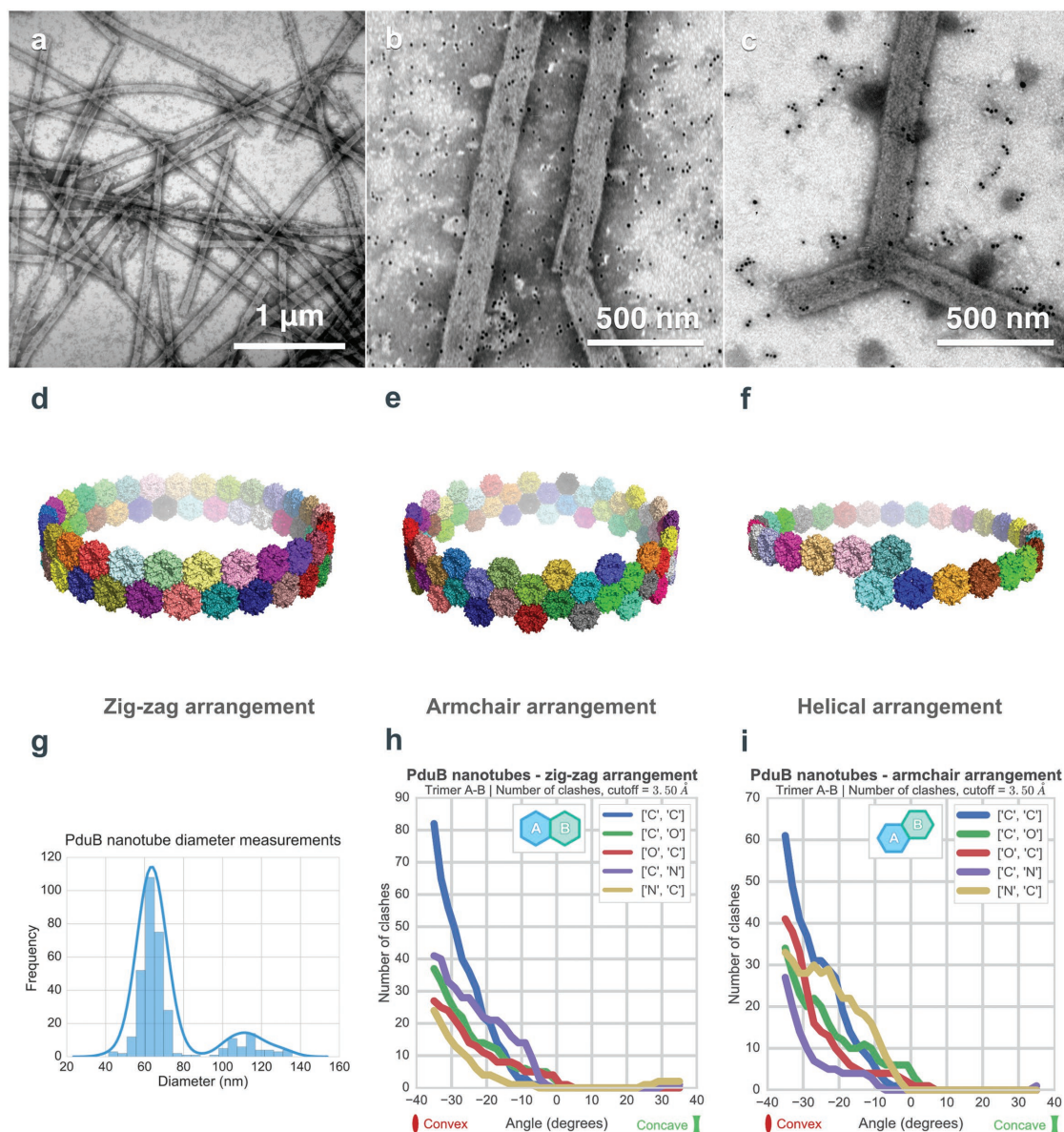


**Figure 4.** PduB nanotubes are larger and show more structural diversity but models suggest the concave surface of PduB also faces out. a) Transmission electron microscopic images of negatively stained PduB *L. reuteri* nanotubes, depicting the large variability in diameter and length, as well as extent of curvature along their lengths. Scale bar 1  $\mu\text{m}$ . b,c) PduB nanotubes labeled with gold nanoparticles in 0.08 and 0.25 M imidazole buffer, respectively. d–f) In silico generated models for PduB nanotubes, depicting the zig-zag, armchair, and helical arrangement respectively. g) Histogram of PduB nanotubes diameters measured ( $n = 336$ ), illustrating their bimodal size distribution. h,i) Number of protein clashes counted at the PduB trimer–trimer interface, as a function of bend angle, for the zig-zag and armchair arrangement, respectively. The concave surface out is again preferred as fewer clashes are seen in this structure.

weight. Cleavage of the His-tag is described in the Supporting Information. Strains and plasmids used are presented in Tables S2 and S3 (Supporting Information), respectively.

**Preparation of Nanotubes:** Nanotubes assembled from PduA and PduB were prepared by dialyzing  $\approx 100 \mu\text{L}$  of a purified solution of the proteins overnight at  $4^\circ\text{C}$ , into 0.05 M Tris-HCl, 0.05 M NaCl, pH 8.0.

**Binding and Release of Nanotubes to Nickel-NTA Magnetic Beads:**  $150 \mu\text{L}$  of PduA nanotube solution ( $\approx 5 \text{ mg mL}^{-1}$ ) was diluted in  $400 \mu\text{L}$  final volume of binding buffer (0.05 M Tris-HCl, 0.05 M NaCl, 0.02 M imidazole, pH 8.0).  $50 \mu\text{L}$  of Qiagen Ni-NTA magnetic agarose beads was added to the nanotube solution, and incubated at  $4^\circ\text{C}$  on a rocker-shaker at slow speed, for a minimum of 30 min. Following incubation, tubes were transferred into a Qiagen single tube magnet for 1 min, and

supernatant transferred to a separate tube. Beads were then washed with  $200 \mu\text{L}$  of 0.02 M imidazole buffer initially, and  $100 \mu\text{L}$  subsequently for buffers of 0.05, 0.15, 0.25, and 0.6 M imidazole. For each wash, supernatant was recovered and a  $20 \mu\text{L}$  sample was taken for loading on to an sodium dodecyl sulfate polyacrylamide gel electrophoresis (SDS PAGE) gel. A final sample of the magnetic beads after washing with 0.6 M imidazole was also taken for loading on the SDS PAGE gel.

**Transmission Electron Microscopy:** Nanotubes were imaged using a JEOL JEM 1230 electron microscope. Samples ( $5 \mu\text{L}$ ) were prepared by depositing onto carbon coated copper grids (Structure Probe, Inc.) for 90 s, followed by 70 s of negative staining using  $5 \mu\text{L}$  of 2.0% phosphotungstic acid (PTA). 5 s of washing using  $5 \mu\text{L}$  of deionized  $\text{H}_2\text{O}$  was carried out after sample deposition and staining. PTA solution

was prepared by dissolving 20 mg of phosphotungstic acid hydrate in 1 mL of deionized H<sub>2</sub>O, followed by incubation at 37 °C overnight. Immediately prior to use, PTA solution was adjusted to pH 7.4 with 10 M NaOH, and filtered through a 0.2 μm micro-syringe filter.

**Nickel-NTA Gold Nanoparticle Binding:** Nanoprobes 5 nm Ni-NTA-Nanogold (gold nanoparticles) solution (AuNPs) was diluted 1:50 in 0.05 M Tris-HCl, 0.05 M NaCl, 0.01–0.5 M imidazole, pH 8.0. TEM grids were prepared with samples of nanotubes (90 s incubation on grid), and subsequently incubated on a 60 μL droplet of the AuNPs for 30 min. Following incubation, the grids were washed twice for 30 s in a droplet of 0.05 M Tris-HCl, 0.05 M NaCl, pH 8.0, before a final wash with ddH<sub>2</sub>O for 10 s. Finally, the grids were stained with filtered 2.0% PTA, pH 7.4 stain for 70 s.

**In Silico Modeling and Algorithms:** Models for nanotubes were generated using custom Python scripts, using the crystal structure of *Salmonella enterica typhimurium* PduA (PDB code: 3NGK) as the building block. For the arrangements, zigzag (Equation (1)) and armchair (Equation (2)), the following equations describe the calculation of the bend angle to give rise to a nanotube of the specified radius, using a hexamer/trimer of the specified width

$$\alpha = \arctan\left(\frac{w}{r_z}\right) \times 2 \quad (1)$$

$$\alpha = \arctan\left(\frac{w \times \frac{3}{8}}{r_a}\right) \times 2 \quad (2)$$

The width of the hexamer/trimer in the orientation required for the arrangement is denoted by,  $w$ , and the radius of the resulting nanotube is denoted by  $r$ .

The helical model was derived by correcting a z-axis rotational offset and subsequently adjusting each successive hexamer/trimer's horizontal offset, such that the horizontal displacement of a full turn of hexamers/trimers corresponded to the pitch of the helix.

**Cloning of TEV Protease and Shell Protein Construct with TEV Cleavage Site:** TEV protease was cloned with an N-terminal hexahistidine tag using Addgene plasmid pRK793 as template (no 8827, S219V mutant). The forward primer included an *AseI* site (underlined) 5'GACATTAATATGCATCATCATCATCATCATGG3' and reverse primer included a *BamHI* site 5'GACGGATCCTTAGCGACGGCGACGACGATTC3'. The polymerase chain reaction (PCR) product was digested *AseI* and *BamHI* and ligated into the *NdeI* and *BamHI* sites of the pETpRha vector to form pETpRha-His-TEV. To insert a TEV cleavage site between mCherry and PduA, PduAB from *C. freundii* was amplified using a PduA forward primer including a *NdeI* site and TEV cleavage sequence 5'CACCATATGGAAAATCTTTATTTTCAAGGTATGCAACAAGAA GCGTTAGGAATGG3' and a PduB reverse primer including a *SpeI* site 5'GGCACTAGTTCAGATGTAGGACGGAC3' using pLysS-mCherry-PduAB as the template. The TEVsite-PduAB PCR product was cloned via *NdeI* and *SpeI* into pLysS-mCherry-PduAB. The mCherry-TEVsite-PduAB fragment was transferred via *SbfI* and *PmlI* into the pLysS-TBAD-mCherry-PduA-BJKNU plasmid to form pLysS-TBAD-mCherry-TEVsite-PduA-BJKNU.

**Culturing Conditions:** DH10β competent cells were cotransformed either with pLysS-TBAD-mCherry-TEVsite-PduA-BJKNU or as a control pLysS-TBAD-mCherry-PduA-BJKNU and pETpRha-His-TEV. To produce the Pdu shell first (pLysS-TBAD-mCherry-TEVsite-PduA-BJKNU) and then the TEV protease (pET-pRha-His-TEV), gene expression was induced with 0.15% w/v L-arabinose for 90 min. To remove L-arabinose cells were washed once in LB medium and resuspended in 25 mL of fresh lysogeny broth (LB) supplemented with 0.2% w/v L-rhamnose for the induction of the TEV protease and cultured for a further 140 min. In positive control samples TEV protease was induced first for 140 min and then shell proteins were produced for 90 min using the same inducer concentrations as above. The cells were not washed as TEV protease was supposed to be coproduced with the shell proteins in this control.

Washing cells added 30 min to the total induction time which is why final harvesting took place after 4 h 20 min. Cells that were not washed were removed from the shaking incubator for 30 min for consistency in sample treatment.

**Fluorescence Microscopy:** Using wide field fluorescence microscopy, whole cells were observed for presence and localization of mCherry signal at the various time points after induction of gene expression. 1 mL cell cultures were harvested, the cells were collected by centrifugation and placed on a 1% agarose-LB pad prepared on a microscope slide and immediately imaged as described before.

**TEM Analysis of Whole Cells:** 20 mL whole cell samples were collected at 4 h 20 min for TEM sample preparation. Samples were ultrathin sectioned on an RMC MT-XL ultramicrotome, collected on uncoated 300 mesh copper grids and stained by incubation in 4.5% uranyl acetate in 1% acetic acid solution for 45 min followed by staining with Reynolds lead citrate for 7 min. Electron microscopy was performed using a JEOL-1230 transmission electron microscope equipped with a Gatan multiscan digital camera operated at an accelerating voltage of 80 kV.

**Western Blot Analysis of TEV Protease and mCherry-PduA Expression:** Samples were collected at 90 min, 140 min, and 4 h 20 min, adjusted to OD<sub>600</sub> = 1 and loaded onto 15% SDS PAGE gels for blotting onto nitrocellulose membranes. Protein production of His-TEV protease and cleavage of mCherry-PduA was probed by incubation of membranes with (i) primary monoclonal anti-poly-histidine antibody (Sigma, H1029) at a dilution of 1:3000 followed by secondary anti mouse IgG, alkaline phosphatase (AP) conjugated at a dilution of 1:5000 and (ii) primary anti-mCherry (Abcam, 1 mg mL<sup>-1</sup>) antibody at 1:2500 followed by secondary anti rabbit IgG antibody, AP-conjugated at 1:5000. Bands were visualized by incubation in substrate 5-bromo-4-chloro-3-indolyl phosphate/nitro blue tetrazolium.

## Supporting Information

Supporting Information is available from the Wiley Online Library or from the author.

## Acknowledgements

This work was supported by the Biotechnology and Biological Sciences Research Council of the UK strategic LoLa Award (BB/M002969/1 to M.J.W. and R.W.P.), BBSRC KTN (BB/M503149/1 to R.W.P.), and by the Leverhulme Trust (ECF-2013-341 to SF). The construct used to produce *L. reuteri* PduB was kindly supplied by Mike B. Prentice (University College Cork) and Mingzhi Liang (University of Kent).

## Conflict of Interest

The authors declare no conflict of interest.

## Keywords

bacterial microcompartment shell proteins, protein nanotubes, self-assembly, transmission electron microscopy

Received: November 16, 2017

Revised: January 26, 2018

Published online: March 24, 2018

[1] T. A. Bobik, G. D. Havemann, R. J. Busch, D. S. Williams, H. C. Aldrich, *J. Bacteriol.* **1999**, *181*, 5967.

- [2] D. Walter, M. Ailion, J. Roth, D. Walter, M. Ailion, J. Roth, *J. Bacteriol.* **1997**, 179, 1013.
- [3] T. O. Yeates, M. C. Thompson, T. a. Bobik, *Curr. Opin. Struct. Biol.* **2011**, 21, 223.
- [4] C. S. Crowley, D. Cascio, M. R. Sawaya, J. S. Kopstein, T. a. Bobik, T. O. Yeates, *J. Biol. Chem.* **2010**, 285, 37838.
- [5] A. Pang, S. Frank, I. Brown, M. J. Warren, R. W. Pickersgill, *J. Biol. Chem.* **2014**, 289, 22377.
- [6] C. R. Noël, F. Cai, C. A. Kerfeld, *Adv. Mater. Interfaces* **2015**, 3, 1.
- [7] J. D. Hunter, *Comput. Sci. Eng.* **2007**, 9, 90.
- [8] S. van der Walt, S. C. Colbert, G. Varoquaux, *Comput. Sci. Eng.* **2011**, 13, 22.
- [9] P. J. A. Cock, T. Antao, J. T. Chang, B. A. Chapman, C. J. Cox, A. Dalke, I. Friedberg, T. Hamelryck, F. Kauff, B. Wilczynski, M. J. L. de Hoon, *Bioinformatics* **2009**, 25, 1422.
- [10] Schrödinger, LLC, *The {PyMOL} Molecular Graphics System, Version~1.8*, New York, NY **2015**.
- [11] V. Reddy, E. Lymar, M. Hu, J. F. Hainfeld, *Microsc. Microanal.* **2005**, 11, 1118.
- [12] P. F. Predki, C. Harford, P. Brar, B. Sarkar, *Biochem. J.* **1992**, 287, 211.
- [13] J. B. Parsons, S. Frank, D. Bhella, M. Liang, M. B. Prentice, D. P. Mulvihill, M. J. Warren, *Mol. Cell* **2010**, 38, 305.
- [14] C. Fan, S. Cheng, Y. Liu, C. M. Escobar, C. S. Crowley, R. E. Jefferson, T. O. Yeates, T. A. Bobik, *Proc. Natl. Acad. Sci. USA* **2010**, 107, 7509.
- [15] J. N. Kinney, A. Salmeen, F. Cai, C. A. Kerfeld, *J. Biol. Chem.* **2012**, 287, 17729.
- [16] T. A. Eastwood, K. Baker, H. R. Brooker, S. Frank, D. P. Mulvihill, *FEBS Lett.* **2017**, 591, 833.
- [17] M. Sutter, M. Faulkner, C. Aussignargues, B. C. Paasch, S. Barrett, C. A. Kerfeld, L.-N. Liu, *Nano Lett.* **2016**, 16, 1590.
- [18] D. Heldt, S. Frank, A. Seyedarabi, D. Ladikis, J. B. Parsons, M. J. Warren, R. W. Pickersgill, *Biochem. J.* **2009**, 423, 199.
- [19] A. Pang, M. J. Warren, R. W. Pickersgill, *Acta Crystallogr., Sect. D: Biol. Crystallogr.* **2011**, 67, 91.
- [20] M. G. Klein, P. Zwart, S. C. Bagby, F. Cai, S. W. Chisholm, S. Heinhorst, G. C. Cannon, C. A. Kerfeld, *J. Mol. Biol.* **2009**, 392, 319.
- [21] A. Pang, M. Liang, M. B. Prentice, R. W. Pickersgill, *Acta Crystallogr., Sect. D: Biol. Crystallogr.* **2012**, 68, 1642.
- [22] M. Sutter, B. Greber, C. Aussignargues, C. A. Kerfeld, *Science* **2017**, 356, 1293.